


An improvement on the Brinson model for shape memory alloys with application to two-dimensional beam element

Saeid Poorasadion¹, Jamal Arghavani¹, Reza Naghdabadi^{1,2} and Saeed Sohrabpour¹

Journal of Intelligent Material Systems and Structures
2014, Vol. 25(15) 1905–1920
© The Author(s) 2013
Reprints and permissions:
sagepub.co.uk/journalsPermissions.nav
DOI: 10.1177/1045389X13512187
jim.sagepub.com


Abstract

In this article, the one-dimensional phenomenological constitutive model originally proposed by Brinson for shape memory alloys is improved to predict asymmetric behavior in tension and compression. We propose an approach that decomposes stress-induced martensite volume fraction into two parts, one in tension and one in compression. Results of numerical examples show reasonable agreement with experimental data. Moreover, we implement the proposed model in a user-defined material subroutine in the nonlinear finite element software ABAQUS/Standard as a two-dimensional Euler–Bernoulli beam element. We simulate several beam problems and a shape memory alloy staple. Regarding the results, the proposed shape memory alloys constitutive model, employed in a two-dimensional beam element, can be used to simulate various shape memory alloys applications in the design and analysis.

Keywords

Shape memory alloy, Brinson model, beam element, asymmetric behavior, user-defined material subroutine

Introduction

Shape memory alloys (SMAs), as a type of smart materials, have unique features known as shape memory effect (SME) and superelasticity (SE). SMAs are being investigated for diverse applications, especially in medical industry as medical stent, staple, orthodontic archwire, and SMA spring (Lagoudas, 2008).

Optimum design of a SMA for specific applications calls for finite element simulations. It is evident that using structural elements (bar, beam, plate, shell) considerably reduces computational cost (central processing unit (CPU) time) when compared to continuum elements. Therefore, structural elements, especially two-dimensional (2D) beam elements, are usually preferred in the early stages of design process. Up to now, there have been several attempts to propose SMA beam element (Auricchio, 2001; Auricchio et al., 2011; Evangelista et al., 2009; Trochu and Qian, 1997; Yang and Xu, 2011). One-dimensional (1D) SMA constitutive models are usually used in the 2D beam element formulation. Phenomenological constitutive models (Arghavani et al., 2010, 2011; Auricchio and Lubliner, 1997; Brinson, 1993; Brocca et al., 2002; Fremond, 1996; Liang and Rogers, 1990; Souza et al., 1998;

Tanaka, 1986) have the characteristics of simplicity and low number of material parameters which make them appropriate candidates for beam element formulation. Among the well-known SMA constitutive models, the one proposed by Brinson in 1993 has extensively been used in the literature (this model is based on the model introduced by Liang and Rogers (1990) that uses a cosine hardening law). Its simple formulation, good agreement with experimental data, and capability to predict material behavior in wide range of temperatures has motivated the current research to develop a 2D beam element based on the 1D Brinson model. While original Brinson model (OBM) is successful in predicting the primary effects (SE and SME), it is unable to capture secondary effects such as internal loops due to

¹Department of Mechanical Engineering, Sharif University of Technology, Tehran, Iran

²Institute for Nanoscience & Nanotechnology, Sharif University of Technology, Tehran, Iran

Corresponding author:

Jamal Arghavani, Department of Mechanical Engineering, Sharif University of Technology, Tehran, Iran.

Email: arghavani@sharif.edu; jamal.arghavani@gmail.com

incomplete phase transformation and asymmetric behavior in tension and compression.

Up to now, there have been several attempts to improve OBM. Chung et al. (2007), Khandelwal and Buravalla (2007), Decastro et al. (2007), and Vigliotti (2010) have improved the transformation kinetics of OBM at low temperatures. In addition, Bekker and Brinson (1998), Buravalla and Khandelwal (2011), and Vigliotti (2010) have proposed algorithms to modify OBM in internal subloops due to incomplete phase transformation. In spite of the existing modifications, OBM has limitations in predicting the asymmetric behavior of SMAs. It is noted that this behavior is of significant importance in the results of SMA beam simulations (Flor et al., 2011; Gall et al., 1999).

To this end, in this study, we focus on the OBM and improve it to predict asymmetric behavior of SMAs in tension and compression. We consider different elastic moduli for austenite, twinned martensite, detwinned martensite in tension, and detwinned martensite in compression. Assuming different stress–temperature slopes as well as different start and finish transformation stresses in tension and compression, a modified phase diagram and corresponding kinetics functions have also been proposed. In addition, different maximum transformation strains in tension and compression are considered. Considering the internal loops, we have utilized the algorithm proposed by Bekker and Brinson (1998). Moreover, we have implemented the proposed model in a user-defined material subroutine (UMAT) in the nonlinear finite element software ABAQUS/Standard v.6.10 to simulate SMA devices based on the 2D Euler–Bernoulli beam element.

The structure of this article is as follows. In section “The SMA phenomenological model,” the OBM is concisely reviewed. An improvement is then proposed which enables the model to predict asymmetric behavior in tension and compression. Based on the improved model, in section “Model predictions under uniaxial loadings,” we solve several examples and compare the results with the experimental data and also models available in the literature. In section “Finite element simulation using beam element,” we implement the proposed model in a UMAT and use the 2D beam element (B23) to simulate SMA devices, including a SMA medical staple. We finally draw conclusions in section “Summary and conclusions.”

The SMA phenomenological model

In this section, the 1D SMA constitutive model originally proposed by Brinson (1993) is first discussed. An improvement is then proposed to describe asymmetric behavior of SMAs.

OBM

In the OBM, the martensite volume fraction (ξ) is decomposed into a stress-induced (ξ_S) and a temperature-induced (ξ_T) part

$$\xi = \xi_S + \xi_T \quad (1)$$

Strain (ε), temperature (T), and the martensite volume fraction (ξ) are considered as state variables. The constitutive equation then takes a differential form as

$$d\sigma = Dd\varepsilon + \Omega_S d\xi_S + \Omega_T d\xi_T + \Theta dT \quad (2)$$

where D and Θ are the elastic modulus and thermoelastic coefficient, respectively, while Ω_T and Ω_S represent temperature-induced and stress-induced transformation coefficients, respectively. Brinson (1993) showed that the temperature-induced transformation coefficient should be zero ($\Omega_T = 0$). The elastic modulus and transformation coefficient are linear functions of the martensite volume fraction, that is

$$D(\xi) = D_a + \xi(D_m - D_a) \quad (3)$$

$$\Omega_S = -\varepsilon_L D(\xi) \quad (4)$$

where D_a and D_m are elastic moduli in austenite and martensite phases, respectively, and ε_L is the maximum transformation strain. Substituting equations (3) and (4) into equation (2) and integrating the results, yields

$$\sigma - \sigma_0 = D(\xi)\varepsilon - D(\xi_0)\varepsilon_0 + \Omega_S(\xi)\xi_S - \Omega_S(\xi_0)\xi_{S0} + \Theta(T - T_0) \quad (5)$$

where ($\sigma_0, \varepsilon_0, \xi_0, \xi_{S0}, T_0$) denote reference values. To describe the transformation process, a phase diagram (Figure 1) was utilized in the OBM. Regarding Figure 1, C_A and C_M are stress–temperature slopes in austenite and martensite phases, respectively. $[A]$ and $[M_T]$ are transformation strips of austenite and twinned martensite phases, respectively, while $[M_{D1}]$, $[M_{D2}]$, and $[M_{D3}]$ are transformation strips of detwinned martensite phase. M_s and M_f are martensite start and finish temperatures, and A_s and A_f are austenite start and finish temperatures, respectively. Moreover, σ_s and σ_f are start and finish transformation stresses, respectively. The unit vectors n^k ($k = A, M_T, M_{D1}, M_{D2}, M_{D3}$) are normal to the corresponding boundary transformation strips. X_0^A and $X_0^{M_T}$ present horizontal distances of transformation strips in austenite and twinned martensite phases, respectively, while $X_0^{M_{D1}}$, $X_0^{M_{D2}}$, and $X_0^{M_{D3}}$ are the vertical distances of transformation strips in the detwinned martensite phase.

According to Figure 1, the martensite volume fraction can be defined at a point (i) of an arbitrary path (L) as follows

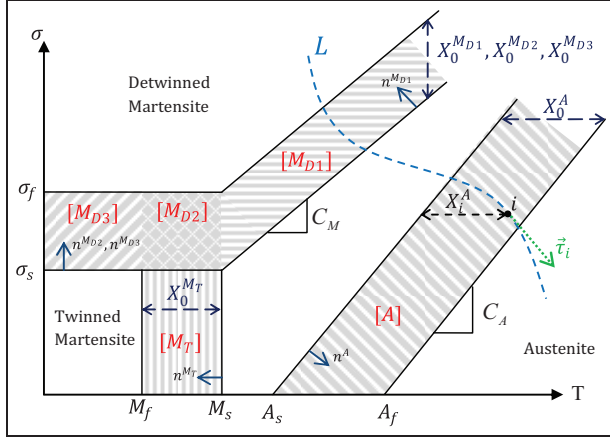


Figure 1. Phase diagram of a SMA (Brinson, 1993).
SMA: shape memory alloy.

$$\xi_i = \begin{cases} f^k(X_i^k, \xi_0) & \text{if } i \in R_k \text{ and } \tau_i \bullet n^k > 0 \\ \xi_0 & \text{otherwise} \end{cases} \quad (6)$$

where R_k is a region, including the point (i), and τ_i is defined as the tangent vector to the path at point (i). The symbol (\bullet) represents the scalar product of vectors. The variables X_i^k ($k = A, M_T, M_{D1}, M_{D2}, M_{D3}$) are the horizontal or vertical distances of point (i) from the start of the transformation strips (these distances are horizontal for austenite and twinned martensite phases and vertical for detwinned martensite phase), as illustrated in Figure 1. Transformation kinetics functions (f^k) are defined in Table 1.

An improvement on the OBM

Experimental results show that SMAs present a tension-compression asymmetric behavior (Flor et al., 2011; Gall et al., 1999). To predict this behavior, we decompose the stress-induced martensite into a tension and a compression part. This approach has already been employed by Fremond (1996), Govindjee and

Kaspar (1999), Wu et al. (1999), and Paiva et al. (2005). Martensite volume fraction (ξ) is therefore decomposed into a stress-induced part in tension (ξ_S^+), a stress-induced part in compression (ξ_S^-), and a temperature-induced part (ξ_T)

$$\xi = \xi_S^+ + \xi_S^- + \xi_T \quad (7)$$

where the superscripts $+$ and $-$ denote, respectively, tension and compression. If $\xi = 0$ (equation (7)), the material is austenite (parent phase). The phase diagram for a SMA is consequently proposed in Figure 2. Utilizing equation (7), we can rewrite equation (2) as

$$d\sigma = Dd\varepsilon + \Omega_S^+ d\xi_S^+ + \Omega_S^- d\xi_S^- + \Omega_T d\xi_T + \Theta dT \quad (8)$$

Constitutive equation with constant material parameters. Assuming the material parameters (D , Ω_S^+ , Ω_S^- , Ω_T , and Θ) to be constant, the constitutive relation can be then easily derived as

$$\sigma - \sigma_0 = D(\varepsilon - \varepsilon_0) + \Omega_S^+ (\xi_S^+ - \xi_{S0}^+) + \Omega_S^- (\xi_S^- - \xi_{S0}^-) + \Omega_T (\xi_T - \xi_{T0}) + \Theta (T - T_0) \quad (9)$$

where ($\sigma_0, \varepsilon_0, \xi_{S0}^+, \xi_{S0}^-, \xi_{T0}, T_0$) denote the reference values. Substituting the initial state (IS) of $IS = (\sigma_0, \varepsilon_0, \xi_{S0}^+, \xi_{S0}^-, \xi_{T0}, T_0) = (0, 0, 0, 0, 0, T_0)$ and the final state (FS) of $FS = (\sigma, \varepsilon, \xi_S^+, \xi_S^-, \xi_T, T) = (0, \varepsilon_L^+, 1, 0, 0, T_0)$ in tension region with $M_s < T_0 < A_s$ into equation (9), we obtain

$$\Omega_S^+ = -\varepsilon_L^+ D \quad (10)$$

where ε_L^+ is a positive number, denoting the maximum transformation strain in tension. Substituting the initial state of $IS = (0, 0, 0, 0, 0, T_0)$ and the final state of $FS = (0, \varepsilon_L^-, 0, 1, 0, T_0)$ in compression region with $M_s < T_0 < A_s$ into equation (9), we also obtain

$$\Omega_S^- = -\varepsilon_L^- D \quad (11)$$

Table 1. Transformation kinetics functions in the original Brinson model (Brinson, 1993) and modifications by Chung et al. (2007) and Khandelwal and Buravalla (2007).

f^k	R_k	$Y_k = \cos\left(\pi \frac{X_0^k}{X_0^k}\right)$	ξ	ξ_T	ξ_S
f^A	[A]	$Y_A = \cos\left(\pi \frac{T - A_s - \sigma/C_A}{A_f - A_s}\right)$	$\frac{\xi_0}{2} (Y_A + 1)$	$\xi_{T0} \frac{\xi}{\xi_0}$	$\xi_{S0} \frac{\xi}{\xi_0}$
f^{M_T}	[M _T]	$Y_{M_T} = \cos\left(\pi \frac{T - M_s}{M_f - M_s}\right)$	$\xi_T + \xi_S$	$\frac{1 - \xi_0}{2} (1 - Y_{M_T}) + \xi_{T0}$	ξ_{S0}
$f^{M_{D1}}$	[M _{D1}]	$Y_{M_{D1}} = \cos\left(\pi \frac{\sigma - \sigma_s - C_M(T - M_s)}{\sigma_f - \sigma_s}\right)$	$\xi_T + \xi_S$	$\xi_{T0} \frac{1 - \xi_S}{1 - \xi_{S0}}$	$\left(\frac{1 - Y_{M_{D1}}}{2}\right) + \xi_{S0} \left(\frac{1 + Y_{M_{D1}}}{2}\right)$
$f^{M_{D2}}$	[M _{D2}]	$Y_{M_{D2}} = Y_{M_{D3}} = \cos\left(\pi \frac{\sigma - \sigma_s}{\sigma_f - \sigma_s}\right)$	$\xi_T + \xi_S$	$\left[\frac{1 - \xi_0}{2} (1 - Y_{M_T}) + \xi_{T0}\right] \times \frac{1 - \xi_S}{1 - \xi_{S0}}$	$\left(\frac{1 - Y_{M_{D2}}}{2}\right) + \xi_{S0} \left(\frac{1 + Y_{M_{D2}}}{2}\right)$
$f^{M_{D3}}$	[M _{D3}]				

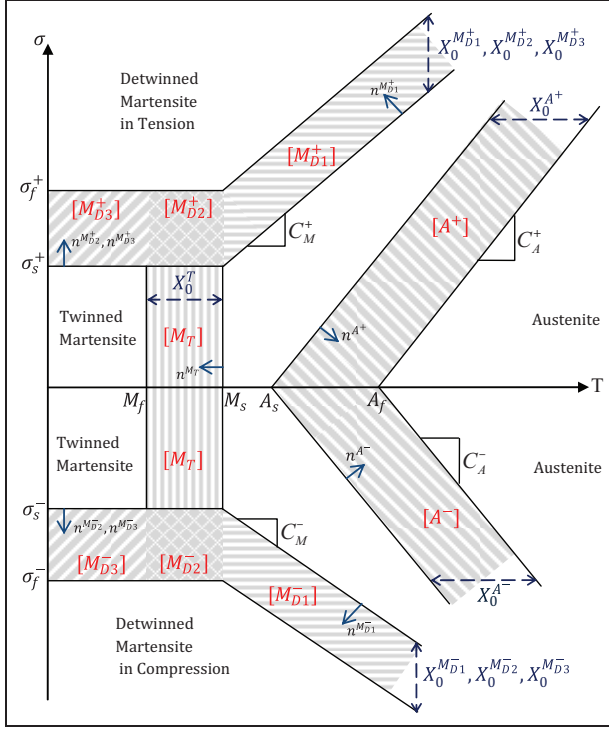


Figure 2. The proposed phase diagram for SMAs in uniaxial tension and compression.
SMA: shape memory alloy.

where ε_L^- is a negative number, denoting the maximum transformation strain in compression. Moreover, considering the initial state of $IS = (0, 0, 0, 0, 1, T_0)$ and the final state of $FS = (0, \varepsilon_L^+, 1, 0, 0, T_0)$ in tension region with $T_0 < A_s$, yields

$$\Omega_T = 0 \quad (12)$$

Thus, the thermomechanical constitutive equation with constant material parameters takes the following form

$$\sigma - \sigma_0 = D(\varepsilon - \varepsilon_0) + \Omega_S^+ (\xi_S^+ - \xi_{S0}^+) + \Omega_S^- (\xi_S^- - \xi_{S0}^-) + \Theta(T - T_0) \quad (13)$$

Constitutive equation with non-constant material parameters. Experimental evidences (Gall et al., 1999) on the modulus of SMAs indicate that it has a strong dependence on the martensite volume fraction. To this end, in this work, we assume different elastic moduli for austenite, twinned martensite, detwinned martensite in tension, and detwinned martensite in compression. Motivated by Brinson (1993), the elastic modulus is then proposed as follows

$$D(\xi) = D_a + \xi_S^+ (D_m^+ - D_a) + \xi_S^- (D_m^- - D_a) + \xi_T (D_m^T - D_a) \quad (14)$$

where D_a and D_m^T are the elastic moduli for fully austenite and fully twinned martensite SMA, respectively, while D_m^+ and D_m^- are the elastic moduli for fully detwinned martensite under tension and compression, respectively. Similar to the process employed in section “Constitutive equation with constant material parameters,” the transformation tensor can be directly related to the elastic modulus and the maximum transformation strain as

$$\begin{aligned} \Omega_S^+ (\xi) &= -\varepsilon_L^+ D(\xi) \\ \Omega_S^- (\xi) &= -\varepsilon_L^- D(\xi) \end{aligned} \quad (15)$$

Furthermore, the material parameter Θ remains constant because its value is extremely small compared to elastic modulus. In a process similar to the one used in derivation of the constant material parameters (section “Constitutive equation with constant material parameters,” equation (12)), it is concluded that $\Omega_T = 0$. Hence, for simplicity, the subscript (s) in Ω_S^+ as well as Ω_S^- is dropped, thus

$$\begin{aligned} \Omega^+ (\xi) &= -\varepsilon_L^+ D(\xi) \\ \Omega^- (\xi) &= -\varepsilon_L^- D(\xi) \end{aligned} \quad (16)$$

Now, equation (8) takes the following form

$$d\sigma = D(\xi)d\varepsilon + \Omega^+ (\xi)d\xi_S^+ + \Omega^- (\xi)d\xi_S^- + \Theta dT \quad (17)$$

Substituting equation (16) into equation (17) and integrating the results, we obtain

$$\begin{aligned} \int d\sigma &= \int D(\xi)d\varepsilon - \int \varepsilon_L^+ [D_a + \xi_S^+ (D_m^+ - D_a) + \xi_S^- (D_m^- - D_a) + \xi_T (D_m^T - D_a)] d\xi_S^+ \\ &\quad - \int \varepsilon_L^- [D_a + \xi_S^+ (D_m^+ - D_a) + \xi_S^- (D_m^- - D_a) + \xi_T (D_m^T - D_a)] d\xi_S^- + \int \Theta dT \end{aligned} \quad (18)$$

Since $D(\xi)$ does not depend on strain, we may conclude

$$\int D(\xi)d\varepsilon = D(\xi)\varepsilon + C(\xi) \quad (19)$$

where $C(\xi)$ is an arbitrary function of martensite volume fraction. We now utilize integration by parts to simplify equation (18) as follows

$$\begin{aligned} \sigma + K = D(\xi)\varepsilon + C(\xi) \\ - \varepsilon_L^+ D_a \xi_S^+ - \varepsilon_L^+ \left((D_m^+ - D_a) \frac{(\xi_S^+)^2}{2} + (D_m^- - D_a) \xi_S^+ \xi_S^- + (D_m^T - D_a) \xi_S^+ \xi_T \right) \\ - \varepsilon_L^- D_a \xi_S^- - \varepsilon_L^- \left((D_m^+ - D_a) \xi_S^- \xi_S^+ + (D_m^- - D_a) \frac{(\xi_S^-)^2}{2} + (D_m^T - D_a) \xi_S^- \xi_T \right) + \Theta T \end{aligned} \quad (20)$$

where K is an arbitrary constant. Utilizing equation (16), we can simplify equation (20) as

$$\begin{aligned} \sigma + K = D(\xi)\varepsilon + \Omega^+ (\xi) \xi_S^+ \\ + \Omega^- (\xi) \xi_S^- + \Theta T + \varepsilon_L^+ (D_m^+ - D_a) \frac{(\xi_S^+)^2}{2} \\ + \varepsilon_L^- (D_m^- - D_a) \frac{(\xi_S^-)^2}{2} + C(\xi) \end{aligned} \quad (21)$$

which is the general solution to the differential equation (17). Equation (21) holds at a reference state $(\sigma_0, \varepsilon_0, \xi_{S0}^+, \xi_{S0}^-, \xi_{T0}, T_0)$. Thus, the unknown constant K , is determined as

$$\begin{aligned} K = D(\xi_0)\varepsilon_0 + \Omega^+ (\xi_0) \xi_{S0}^+ + \Omega^- (\xi_0) \xi_{S0}^- \\ + \Theta T_0 + \varepsilon_L^+ (D_m^+ - D_a) \frac{(\xi_{S0}^+)^2}{2} \\ + \varepsilon_L^- (D_m^- - D_a) \frac{(\xi_{S0}^-)^2}{2} + C(\xi_0) - \sigma_0 \end{aligned} \quad (22)$$

Substituting equation (22) into equation (21), we obtain

$$\begin{aligned} \sigma - \sigma_0 = D(\xi)\varepsilon - D(\xi_0)\varepsilon_0 + \Omega^+ (\xi) \xi_S^+ - \Omega^+ (\xi_0) \xi_{S0}^+ \\ + \Omega^- (\xi) \xi_S^- - \Omega^- (\xi_0) \xi_{S0}^- \\ + \Theta(T - T_0) + \varepsilon_L^+ (D_m^+ - D_a) \left[\frac{(\xi_S^+)^2}{2} - \frac{(\xi_{S0}^+)^2}{2} \right] \\ + \varepsilon_L^- (D_m^- - D_a) \left[\frac{(\xi_S^-)^2}{2} - \frac{(\xi_{S0}^-)^2}{2} \right] + C(\xi) - C(\xi_0) \end{aligned} \quad (23)$$

We now consider a uniaxial tension loading as well as a uniaxial compression loading. In the first case, we use the initial state of $IS = (0, 0, 0, 0, 0, T_0)$ and reach the final state of $FS = (0, \varepsilon_L^+, \xi_S^+, 0, 0, T_0)$, where T_0 is between M_s and A_s . It then yields

$$\varepsilon_L^+ (D_m^+ - D_a) \frac{(\xi_S^+)^2}{2} + C(\xi) = 0 \quad (24)$$

Similarly, for the compression case of equation (24) with $IS = (0, 0, 0, 0, 0, T_0)$ and $FS = (0, \varepsilon_L^-, \xi_S^-, 0, 0, T_0)$, where T_0 is between M_s and A_s , we obtain

$$\varepsilon_L^- (D_m^- - D_a) \frac{(\xi_S^-)^2}{2} + C(\xi) = 0 \quad (25)$$

Considering equations (24) and (25), the unknown function $C(\xi)$ can be defined as

$$C(\xi) = -\varepsilon_L^+ (D_m^+ - D_a) \frac{(\xi_S^+)^2}{2} - \varepsilon_L^- (D_m^- - D_a) \frac{(\xi_S^-)^2}{2} \quad (26)$$

Substituting equation (26) into equation (23), constitutive equation for asymmetric behavior of SMAs with non-constant material parameters takes the following form

$$\begin{aligned} \sigma - \sigma_0 = D(\xi)\varepsilon - D(\xi_0)\varepsilon_0 + \left(\Omega^+ (\xi) \xi_S^+ + \Omega^- (\xi) \xi_S^- \right) \\ - \left(\Omega^+ (\xi_0) \xi_{S0}^+ + \Omega^- (\xi_0) \xi_{S0}^- \right) + \Theta(T - T_0) \end{aligned} \quad (27)$$

The martensite volume fractions can be defined at a point (i) of an arbitrary path as

$$\xi_i = \begin{cases} F^k(X_i^k, \xi_0) & \text{if } i \in R_k \text{ and } \tau_i \bullet n^k > 0 \\ \xi_0 & \text{otherwise} \end{cases} \quad (28)$$

Transformation kinetics functions (F^k) are introduced in Table 2.

Model predictions under uniaxial loadings

In this section, several numerical examples are presented. Predictions of the proposed model are compared with experimental data available in the literature. To simulate examples based on the proposed model, the material parameters (elastic moduli, transformation stresses, stress-temperature slopes, transformation strains, thermoelastic modulus, and transformation temperatures) are required. The transformation temperatures are usually reported in the literature, but other parameters can be calibrated from uniaxial loading in tension and compression at various temperatures (two temperatures are required). Since available experimental data in the literature are usually for tension at several temperatures or tension and compression at just one temperature, we use best fit method to adopt material parameters where needed.

Example 1: asymmetry in tension and compression

A specimen of $Ti - Ni$ is subjected to uniaxial loading-unloading in tension and compression. Temperature remains constant at 22°C, which is below A_s . The material parameters presented in Table 3 have been adopted from the experimental data reported by Gall et al.

Table 2. Transformation kinetics functions of the proposed asymmetric SMA constitutive model.

F^k	R_k	$Y_k = \cos\left(\pi \frac{\chi_k^+}{\chi_0^+}\right)$	ξ	ξ_T	ξ_S^+	ξ_S^-
F^{A^+}	$[A^+]$	$Y_{A^+} = \cos\left(\pi \frac{T-A_s-\sigma/C_A^+}{A_f-A_s}\right)$	$\frac{\xi_0}{2}(Y_{A^+} + 1)$	$\xi_{T0} \frac{\xi}{\xi_0}$	$\xi_{S0}^+ \frac{\xi}{\xi_0}$	$\xi_{S0}^- \frac{\xi}{\xi_0}$
F^{M_T}	$[M_T]$	$Y_{M_T} = \cos\left(\pi \frac{T-M_s}{M_f-M_s}\right)$	$\xi_T + \xi_S^+ + \xi_S^-$	$\frac{1-\xi_0}{2}(1 - Y_{M_T}) + \xi_{T0}$	ξ_{S0}^+	ξ_{S0}^-
$F^{M_{D1}^+}$	$[M_{D1}^+]$	$Y_{M_{D1}^+} = \cos\left(\pi \frac{\sigma - \sigma_s^+ - C_M^+(T-M_s)}{\sigma_f^+ - \sigma_s^+}\right)$	$\xi_T + \xi_S^+ + \xi_S^-$	$\xi_{T0} \frac{1-\xi^+}{1-\xi_{S0}^+}$	$\left(\frac{1-Y_{M_{D1}^+}}{2}\right) + \xi_{S0}^+$	$\left(\frac{1-\xi^+}{2}\right) + \xi_{S0}^-$
$F^{M_{D2}^+}$	$[M_{D2}^+]$	$Y_{M_{D2}^+} = \cos\left(\pi \frac{\sigma - \sigma_s^+}{\sigma_f^+ - \sigma_s^+}\right)$	$\xi_T + \xi_S^+ + \xi_S^-$	$\left[\frac{1-\xi_0}{2}(1 - Y_{M_T}) + \xi_{T0}\right] \times \frac{1-\xi^+}{1-\xi_{S0}^+}$	$\left(\frac{1-Y_{M_{D2}^+}}{2}\right) + \xi_{S0}^+$	$\left(\frac{1-\xi^+}{2}\right) + \xi_{S0}^-$
$F^{M_{D3}^+}$	$[M_{D3}^+]$	$Y_{M_{D3}^+} = \cos\left(\pi \frac{T-A_s-\sigma/C_A^+}{A_f-A_s}\right)$	$\xi_T + \xi_S^+ + \xi_S^-$	$\xi_{T0} \frac{1-\xi^+}{1-\xi_{S0}^+}$	ξ_{S0}^+	ξ_{S0}^-
F^{A^-}	$[A^-]$	$Y_{A^-} = \cos\left(\pi \frac{T-A_s-\sigma/C_A^-}{A_f-A_s}\right)$	$\frac{\xi_0}{2}(Y_{A^-} + 1)$	$\xi_{T0} \frac{\xi}{\xi_0}$	$\xi_{S0}^+ \frac{\xi}{\xi_0}$	$\xi_{S0}^- \frac{\xi}{\xi_0}$
$F^{M_{D1}^-}$	$[M_{D1}^-]$	$Y_{M_{D1}^-} = \cos\left(\pi \frac{\sigma - \sigma_s^- - C_M^-(T-M_s)}{\sigma_f^- - \sigma_s^-}\right)$	$\xi_T + \xi_S^+ + \xi_S^-$	$\xi_{T0} \frac{1-\xi^-}{1-\xi_{S0}^-}$	$\left(\frac{1-Y_{M_{D1}^-}}{2}\right) + \xi_{S0}^+$	$\left(\frac{1-\xi^-}{2}\right) + \xi_{S0}^-$
$F^{M_{D2}^-}$	$[M_{D2}^-]$	$Y_{M_{D2}^-} = \cos\left(\pi \frac{\sigma - \sigma_s^-}{\sigma_f^- - \sigma_s^-}\right)$	$\xi_T + \xi_S^+ + \xi_S^-$	$\left[\frac{1-\xi_0}{2}(1 - Y_{M_T}) + \xi_{T0}\right] \times \frac{1-\xi^-}{1-\xi_{S0}^-}$	$\left(\frac{1-Y_{M_{D2}^-}}{2}\right) + \xi_{S0}^+$	$\left(\frac{1-\xi^-}{2}\right) + \xi_{S0}^-$
$F^{M_{D3}^-}$	$[M_{D3}^-]$	$Y_{M_{D3}^-} = \cos\left(\pi \frac{T-A_s-\sigma/C_A^-}{A_f-A_s}\right)$	$\xi_T + \xi_S^+ + \xi_S^-$	$\xi_{T0} \frac{1-\xi^-}{1-\xi_{S0}^-}$	ξ_{S0}^+	ξ_{S0}^-

(1999). In Figure 3, the predictions of the proposed model, the digitized data related to the model presented by Zaki (2010), and experimental data reported by Gall et al. (1999) have been compared. It is observed that the predictions of the proposed model are in a good agreement with the experimental data. Moreover, the experimental data verify that the moduli of martensite SMA are clearly different in tension and compression. We remark that the model proposed by Zaki (2010) does not consider different elastic modulus in tension and compression. It seems that, if different moduli are considered in Zaki (2010), the predictions can be improved.

Example 2: uniaxial tension–compression test

Regarding Tokuda et al. (1999), the specimen of $Cu - Al - Zn - Mn$ is subjected to tension–compression load at low temperature -30°C . In this process, the maximum loading in tension and compression are equal. The material parameters presented in Table 4 have been adopted from experimental data reported by Tokuda et al. (1999). Stress versus strain diagram of the proposed model, and the experimental data are compared in Figure 4. In addition, the prediction of the proposed model when the material parameters are assumed to be same in tension and compression (symmetric model) is also represented in Figure 4. This comparison shows that the proposed asymmetric SMA constitutive model predicts more accurate behavior when compared to the symmetric one.

Moreover, uniaxial loading–unloading at four different constant temperatures of -55°C , -35°C , -25°C , and -15°C up to the maximum stress value of 250 MPa are also considered. As shown in Figure 5, the proposed model is able to predict the characteristics of hysteresis loops of SMAs both in tension and compression, especially at temperatures below A_s . In addition, start and finish transformation stresses increase with temperature, as experimentally observed in the literature (Lagoudas, 2008; Tokuda et al., 1999).

Finite element simulation using beam element

A beam element based on the proposed model is discussed in the following. The element, schematically illustrated in Figure 6, has two nodes and three degrees of freedom per node ($d_{ix}, d_{iy}, \phi_{iz}$). Moreover, the element is subjected to axial, transverse, and bending loadings.

Following the Euler–Bernoulli beam theory, the plane cross-sections initially normal to the beam axis remain plane and normal to the beam axis. Axial (u) and transversal (v) displacements in the beam take the following form

$$\begin{cases} u = u_0(x) - y \frac{dv_0(x)}{dx} \\ v = v_0(x) \end{cases} \quad (29)$$

Table 3. Material parameters adopted for Gall et al. (1999) experiment.

Property	Unit	Value
Moduli	[GPa]	$D_m^+ = 11$, $D_m^- = 80$, $D_m^T = 11$, $D_a = 39$
Transformation stresses	[MPa]	$\sigma_s^+ = 60$, $\sigma_f^+ = 160$, $\sigma_s^- = 5$, $\sigma_f^- = 260$
Stress–temperature slopes	[MPa/°C]	$C_M^+ = 8$, $C_A^+ = 3.5$, $C_M^- = 5$, $C_A^- = 3.5$
Transformation strain	[–]	$\varepsilon_L^+ = 0.034$, $\varepsilon_L^- = -0.021$
Thermoelastic modulus	[MPa/°C]	$\Theta = 0.55$
Transformation temperatures	[°C]	$M_f = -10$, $M_s = -3$, $A_s = 30$, $A_f = 45$

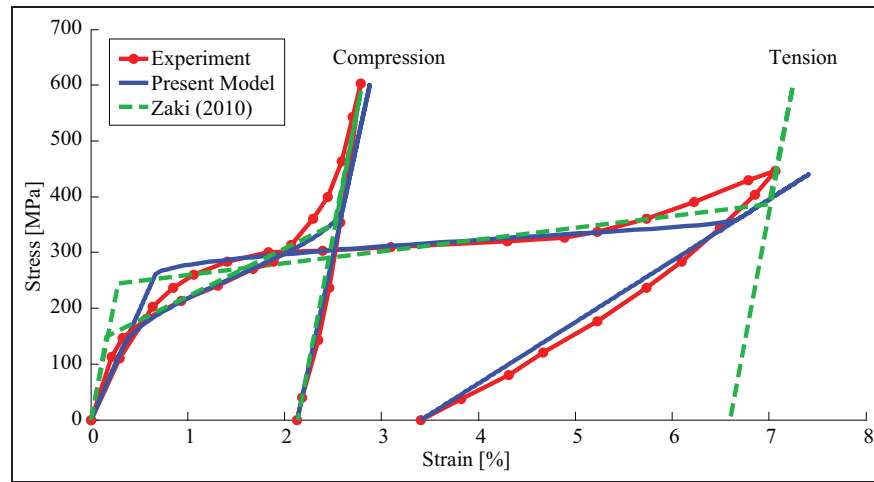


Figure 3. Comparison between the model predictions and the experimental data (Gall et al., 1999).

Table 4. Material parameters adopted for Tokuda et al. (1999) experiment.

Property	Unit	Value
Moduli	[GPa]	$D_m^+ = 26$, $D_m^- = 33$, $D_m^T = 26$, $D_a = 34.9$
Transformation stresses	[MPa]	$\sigma_s^+ = 70$, $\sigma_f^+ = 188$, $\sigma_s^- = 0$, $\sigma_f^- = 220$
Stress–temperature slopes	[MPa/°C]	$C_M^+ = 1$, $C_A^+ = 3$, $C_M^- = 0.2$, $C_A^- = 3$
Transformation strain	[–]	$\varepsilon_L^+ = 0.016$, $\varepsilon_L^- = -0.0146$
Thermoelastic modulus	[MPa/°C]	$\Theta = 0.55$
Transformation temperatures	[°C]	$M_f = -55$, $M_s = -35$, $A_s = -30$, $A_f = -15$

where $u_0(x)$ and $v_0(x)$ are the displacement components of the neutral axis. Using equation (29), we obtain the nonzero strain component as follows

$$\varepsilon = \frac{du_0(x)}{dx} - y \frac{d^2v_0(x)}{dx^2} \quad (30)$$

The details of finite element formulation are given in Appendix 1. Finite element simulation of the SMA beam is carried out in ABAQUS/Standard v.6.10. To determine the integration of stiffness matrix (equation (49) in Appendix 1), internal and external forces (equation (46) in Appendix 1), three gauss points are used in ABAQUS, which allows user implementations of

constitutive equations through a FORTRAN subroutine called UMAT.

Stress update, tangent matrix derivation, and solution algorithm

The solution algorithm of the subroutine UMAT is expressed in this section. To calculate stress, knowing the strain and temperature, the proposed constitutive equation (equation (27)) can be expressed as a function of stress

$$F(\sigma) = D(\xi)\varepsilon - D(\xi_0)\varepsilon_0 + \left(\Omega^+(\xi)\xi_s^+ + \Omega^-(\xi)\xi_s^- \right) - \left(\Omega^+(\xi_0)\xi_{s0}^+ + \Omega^-(\xi_0)\xi_{s0}^- \right) + \Theta(T - T_0) - \sigma + \sigma_0 \quad (31)$$

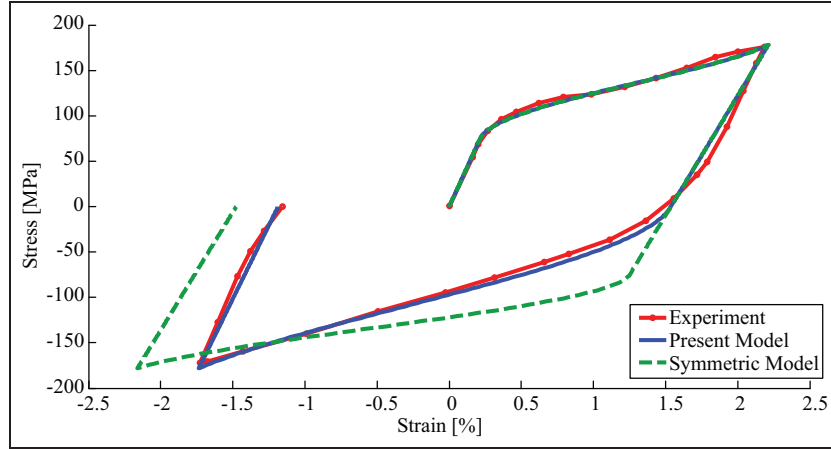


Figure 4. Comparison between the model predictions and the experimental data (Tokuda et al., 1999).

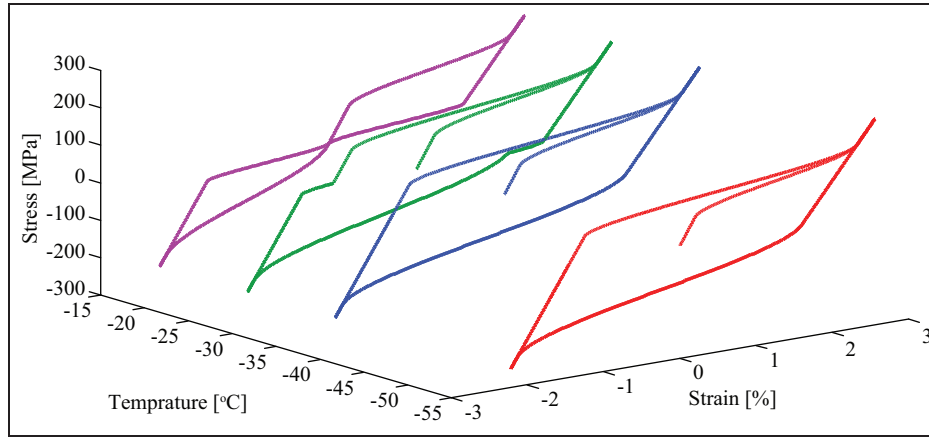


Figure 5. The model predictions for tension–compression uniaxial loading at constant temperatures.

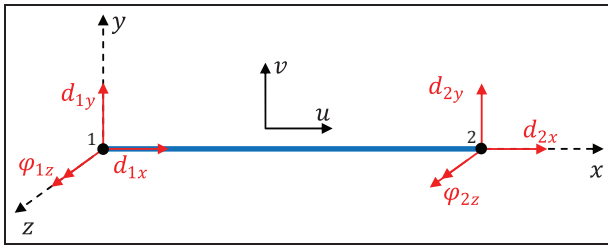


Figure 6. Beam element based on Euler–Bernoulli beam theory.

To solve equation (31), we use Newton–Raphson method. Therefore, the derivative of equation (31) is required

$$\frac{dF(\sigma)}{d\sigma} = \left(\frac{d}{d\sigma}(D(\xi)) \right) \varepsilon + \left(\Omega^+(\xi) \frac{d\xi_s^+}{d\sigma} + \Omega^-(\xi) \frac{d\xi_s^-}{d\sigma} \right) - \left(\varepsilon_L^+ \xi_s^+ + \varepsilon_L^- \xi_s^- \right) \frac{d}{d\sigma}(D(\xi)) - 1 \quad (32)$$

Utilizing equation (14), the derivative of the elastic modulus can be expressed as

$$\begin{aligned} \frac{d}{d\sigma}(D(\xi)) &= \frac{\partial D(\xi)}{\partial \xi_s^+} \frac{d\xi_s^+}{d\sigma} + \frac{\partial D(\xi)}{\partial \xi_s^-} \frac{d\xi_s^-}{d\sigma} + \frac{\partial D(\xi)}{\partial \xi_T} \frac{d\xi_T}{d\sigma} \\ &= (D_m^+ - D_a) \frac{d\xi_s^+}{d\sigma} + (D_m^- - D_a) \frac{d\xi_s^-}{d\sigma} + (D_m^T - D_a) \frac{d\xi_T}{d\sigma} \\ &= D_m^+ \frac{d\xi_s^+}{d\sigma} + D_m^- \frac{d\xi_s^-}{d\sigma} + D_m^T \frac{d\xi_T}{d\sigma} - D_a \frac{d\xi}{d\sigma} \end{aligned} \quad (33)$$

Substituting equation (33) into equation (32), we obtain

$$\begin{aligned} \frac{dF(\sigma)}{d\sigma} &= \left(\varepsilon - \varepsilon_L^+ \xi_s^+ - \varepsilon_L^- \xi_s^- \right) \\ &\quad \left[D_m^+ \frac{d\xi_s^+}{d\sigma} + D_m^- \frac{d\xi_s^-}{d\sigma} + D_m^T \frac{d\xi_T}{d\sigma} - D_a \frac{d\xi}{d\sigma} \right] \\ &\quad + \Omega^+(\xi) \frac{d\xi_s^+}{d\sigma} + \Omega^-(\xi) \frac{d\xi_s^-}{d\sigma} - 1 \end{aligned} \quad (34)$$

To define the tangent matrix, assuming $dT = 0$, the differential equation (27) can be derived as

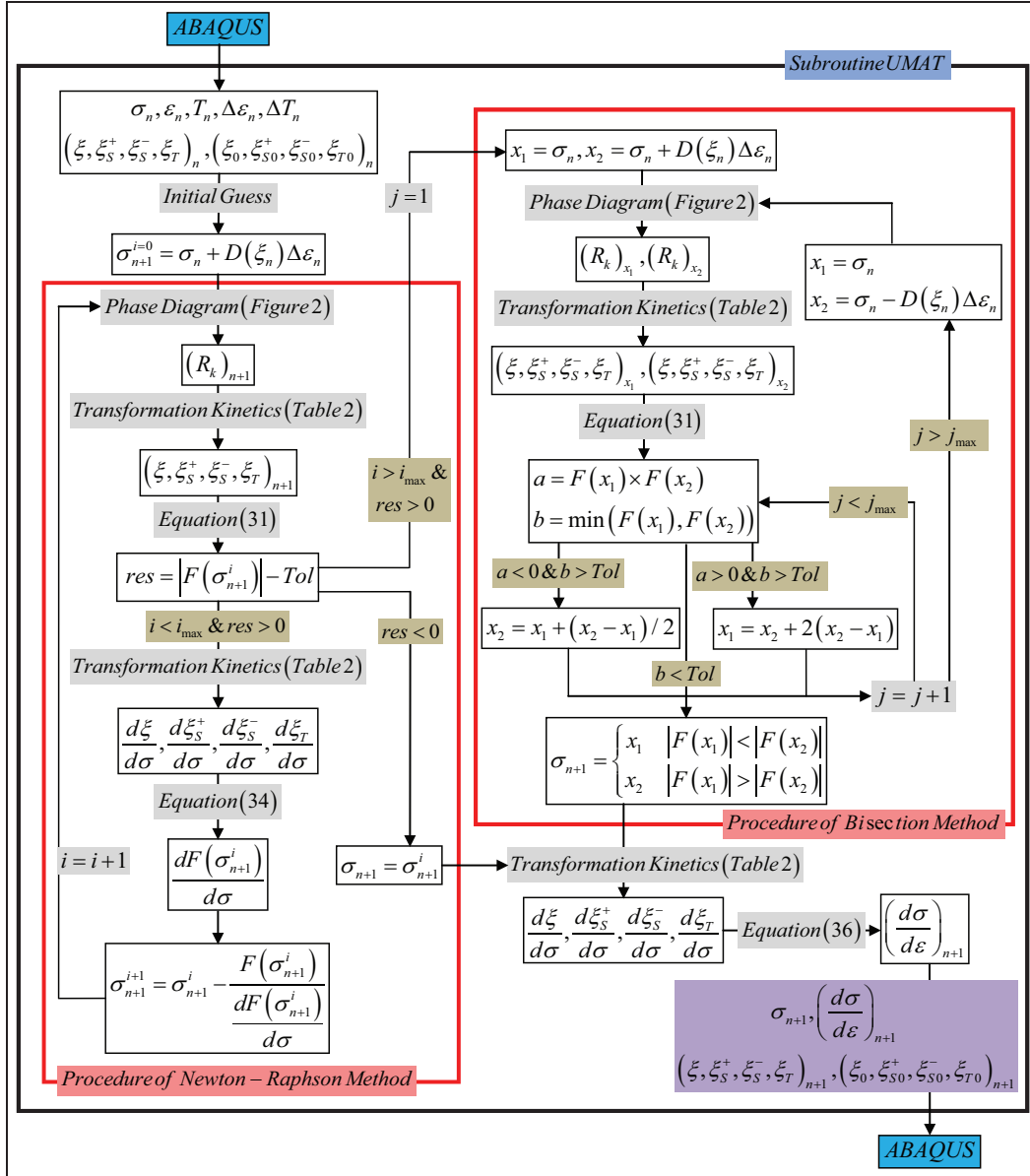


Figure 7. Solution algorithm for the proposed SMA constitutive model.
SMA: shape memory alloy.

$$\begin{aligned}
 d\sigma = & \left(\frac{d}{d\sigma} (D(\xi)) d\sigma \right) \varepsilon + D(\xi) d\varepsilon \\
 & + \left(\Omega^+(\xi) \frac{d\xi_s^+}{d\sigma} + \Omega^-(\xi) \frac{d\xi_s^-}{d\sigma} \right) d\sigma \quad (35) \\
 & - \left(\varepsilon_L^+ \xi_s^+ + \varepsilon_L^- \xi_s^- \right) \frac{d}{d\sigma} (D(\xi)) d\sigma
 \end{aligned}$$

Substituting equation (33) into equation (35), the tangent matrix (C) can be expressed as

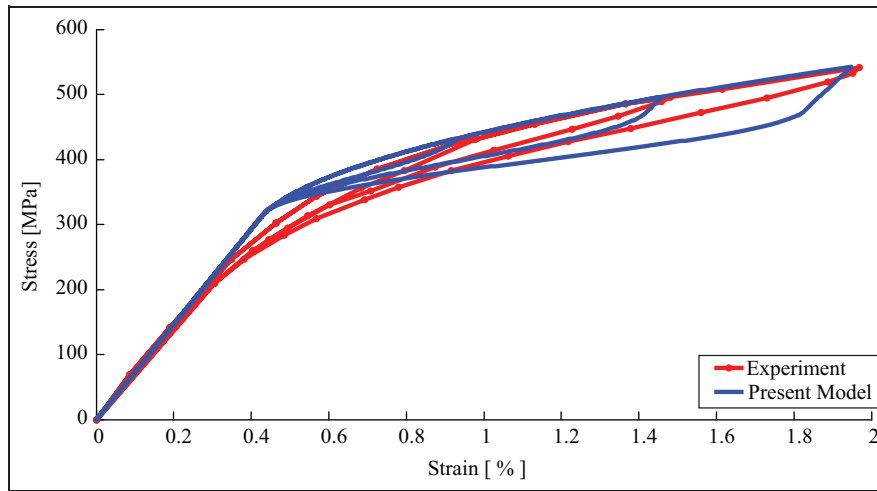
$$C = \frac{d\sigma}{d\varepsilon} = \frac{D(\xi)}{1 - \left(\varepsilon - \varepsilon_L^+ \xi_s^+ - \varepsilon_L^- \xi_s^- \right) \left[D_m^+ \frac{d\xi_s^+}{d\sigma} + D_m^- \frac{d\xi_s^-}{d\sigma} + D_m^T \frac{d\xi_T}{d\sigma} - D_a \frac{d\xi}{d\sigma} \right] - \Omega^+(\xi) \frac{d\xi_s^+}{d\sigma} - \Omega^-(\xi) \frac{d\xi_s^-}{d\sigma}} \quad (36)$$

The derivatives of the martensite volume fractions ($d\xi/d\sigma$, $d\xi_s^+/d\sigma$, $d\xi_s^-/d\sigma$, and $d\xi_T/d\sigma$) are obtained by taking derivatives of the equations presented in Table 2.

The solution algorithm for the proposed SMA constitutive model has been presented in Figure 7. We define stress (equation (27)) and tangent matrix (equation (36)), knowing the strain (ε_{n+1}) and temperature (T_{n+1}) at time t_{n+1} and the stress (σ_n), strain (ε_n), temperature (T_n), and martensite volume fractions

Table 5. Material parameters adopted for Gillet et al. (1998) experiment.

Property	Unit	Value
Moduli	[GPa]	$D_m^+ = 10, D_m^- = 10, D_m^T = 10, D_a = 73.2$
Transformation stresses	[MPa]	$\sigma_s^+ = 60, \sigma_f^+ = 720, \sigma_s^- = 60, \sigma_f^- = 440$
Stress–temperature slopes	[MPa/°C]	$C_M^+ = 2, C_A^+ = 2.9, C_M^- = 2, C_A^- = 2.3$
Transformation strain	[–]	$\varepsilon_L^+ = 0.035, \varepsilon_L^- = -0.03$
Thermoelastic modulus	[MPa/°C]	$\Theta = 0.55$
Transformation temperatures	[°C]	$M_f = -110, M_s = -105, A_s = -104, A_f = -90$

**Figure 8.** Comparison between the model prediction and the experimental data (Gillet et al., 1998) for loading–unloading test at 19.3°C.

$(\xi, \xi_S^+, \xi_S^-, \xi_T)_n, (\xi_0, \xi_{S0}^+, \xi_{S0}^-, \xi_{T0})_n$ at time t_n . To solve nonlinear equation (27), we employ the Newton–Raphson method. In addition, we use the Bisection method when the Newton–Raphson method fails to converge. Regarding Figure 7, Tol denotes tolerance of convergence in Newton–Raphson and Bisection methods. Moreover, i_{\max} and j_{\max} are the maximum number of iterations used in the Newton–Raphson and Bisection methods, respectively.

Example 1: three-point bending

In this example, a three-point bending problem is studied with specimen of *Cu–Al–Be* alloy at 19.3°C reported by Gillet et al. (1998). The material parameters (reported in Table 5) are identified using the experimental data reported by Gillet et al. (1998) for loading–unloading cycle tests at room temperature (19.3°C). Figure 8 shows the model predictions for these tests.

After material parameter identification, the three-point bending beam problem is simulated at constant temperature of 19.3°C. In this problem, the beam is simply supported on two outer points and the parent

phase of the beam is austenite. The beam has a rectangular cross section of width 2.9 mm, thickness 0.95 mm, and length of 49.92 mm. A force of 26 N is applied in the middle section of the beam and is then unloaded.

The prediction of the proposed model with 50 beam elements (B23), shown in Figure 9, has a good agreement with the experimental data reported by Gillet et al. (1998). In addition, the prediction of the symmetric model is compared with the experimental data. This comparison shows that the proposed asymmetric SMA constitutive model reveals better agreements with the experimental bending data than the symmetric one.

Example 2: cantilever beam

A cantilever beam is studied at two different temperatures with specimen of *Ti–Ni*. The material parameters presented in Table 6 are identified using the experimental data reported by Flor et al. (2006) for loading–unloading cycle tests at three temperatures (46.5°C, 65°C, and 100°C). Figure 10 shows the model predictions for these tests.

The beam, anchored at one end, is subjected to a force (F) at another end. It has a circular cross section

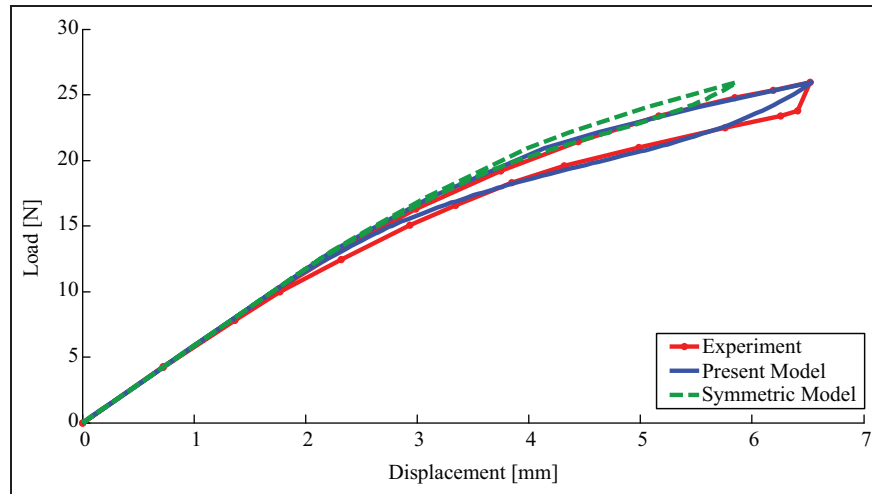


Figure 9. Comparison between the model predictions and the experimental data (Gillet et al., 1998) for three-point bending test.

Table 6. Material parameters adopted for Flor et al. (2006) experiment.

Property	Unit	Value
Moduli	[GPa]	$D_m^+ = 30, D_m^- = 40, D_m^T = 35, D_a = 76.8$
Transformation stresses	[MPa]	$\sigma_s^+ = 50, \sigma_f^+ = 90, \sigma_s^- = 103, \sigma_f^- = 104$
Stress–temperature slopes	[MPa/°C]	$C_M^+ = 7.8, C_A^+ = 4, C_M^- = 3.38, C_A^- = 4$
Transformation strain	[–]	$\varepsilon_L^+ = 0.074, \varepsilon_L^- = -0.045$
Thermoelastic modulus	[MPa/°C]	$\Theta = 0.55$
Transformation temperatures	[°C]	$M_f = 24, M_s = 49, A_s = 75, A_f = 82.5$

with diameter of 1 mm and length of 60 mm. At constant temperature of 50°C, which is below A_s , the prediction of the proposed model for $F = 0.31\text{ N}$ with 20 beam elements (B23) as well as the digitized data related to the model presented by Flor et al. (2011) (referred to as FU (2011)) and experimental data reported by Flor et al. (2011) are compared in Figure 11. A good qualitative correlation between the experimental data and the prediction of the proposed model can be observed.

In the second study, temperature during loading is 85°C, which is above A_f . The prediction of the proposed asymmetric SMA constitutive model, the prediction of the symmetric model, and the experimental data reported by Flor et al. (2011), for $F = 1.15\text{ N}$, are compared in Figure 12. The results show that the asymmetric behavior in tension and compression has considerable effect on the response of the SMA wire subjected to bending.

Example 3: SMA staple

A Nitinol SMA staple (Figure 13) is used for fixing two bones. This device consists of two legs and is used in idiopathic scoliosis treatment by vertebral body stapling

(Jaber et al., 2008). Evaluation of the force applied to staple legs to make them nearly vertical after elastic unloading, is a major concern in staple design. We now simulate the staple presented by Jaber et al. (2008) and determine the mentioned force (Figure 14).

The material properties used in the simulation are reported in Table 7 (Jaber et al., 2008). The staple is subjected to horizontal forces at points A and B (Figure 14) at temperature of 15°C (below A_s). The legs of the staple are loaded until they become nearly vertical after elastic unloading. To recover the initial shape (austenite phase), the temperature is increased to 37°C (human body temperature). The required load is determined as $F = 24.2\text{ N}$ with 40 beam elements (B23), while Jaber et al. (2008) have reached $F = 28\text{ N}$ with a three-dimensional (3D) beam element based on finite strain description. It is observed that the 2D beam element based on the proposed model can be effectively used in the design of SMA devices. The undeformed geometry as well as geometries after loading and after unloading of the staple is shown in Figure 15. Moreover, the force–displacement–temperature diagram at point A is shown in Figure 16.

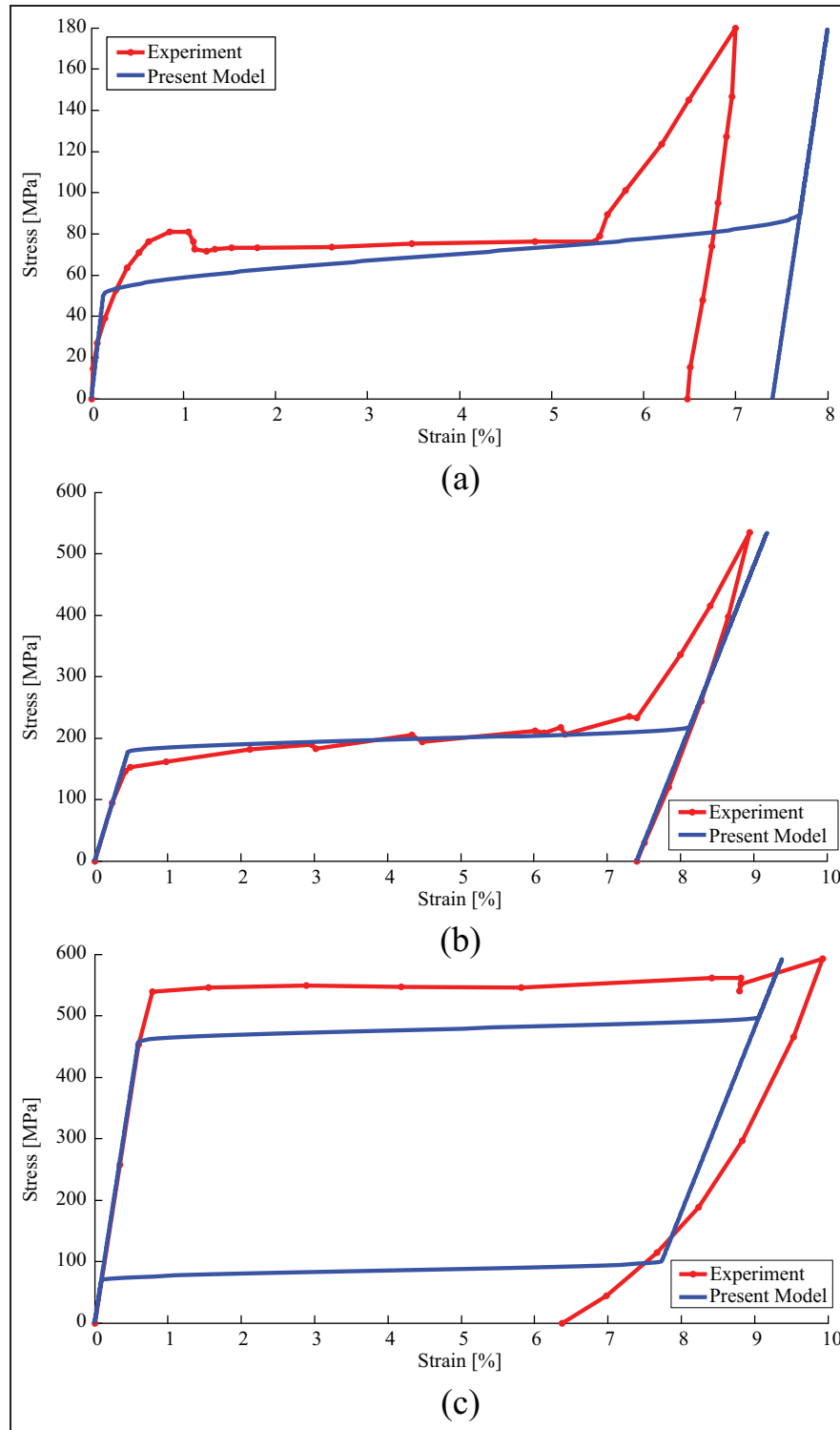


Figure 10. Comparison between the model prediction and the experimental data (Flor et al., 2006): (a) 46.5 °C, (b) 65 °C, and (c) 100 °C.²

Summary and conclusion

In this study, we present an improvement on the one-dimensional phenomenological constitutive model originally proposed by Brinson to predict the asymmetric

behavior of SMAs in tension and compression. To this end, stress-induced martensite volume fraction is decomposed into two parts, one in tension and one in compression. Comparison of the proposed model

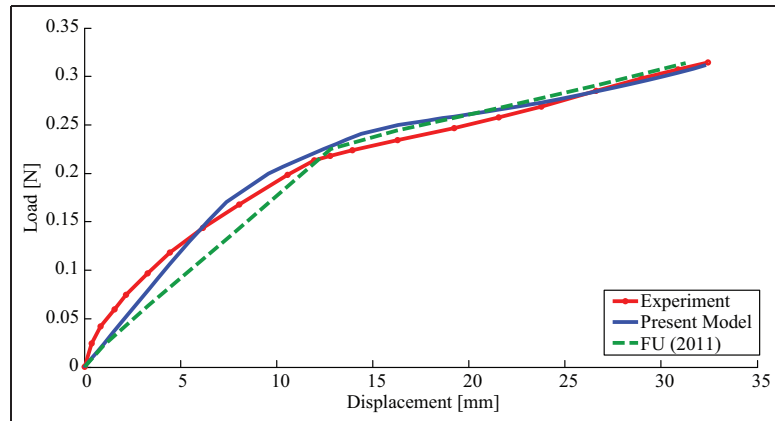


Figure 11. Comparison between the model predictions and the experimental data (Flor et al., 2011) at 50 °C for the cantilever beam.

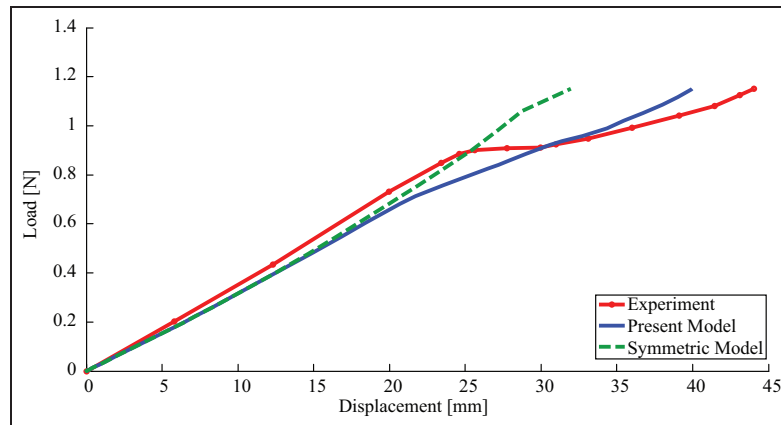


Figure 12. Comparison between the model predictions and the experimental data (Flor et al., 2011) at 85 °C for the cantilever beam.

Table 7. Material parameters considered by Jaber et al. (2008).

Property	Unit	Value
Moduli	[GPa]	$D_m^+ = 70$, $D_m^- = 70$, $D_m^T = 70$, $D_a = 70$
Transformation stresses	[MPa]	$\sigma_s^+ = 100$, $\sigma_f^+ = 170$, $\sigma_s^- = 100$, $\sigma_f^- = 170$
Stress–temperature slopes	[MPa/°C]	$C_M^+ = 5$, $C_A^+ = 5$, $C_M^- = 5$, $C_A^- = 5$
Transformation strain	[–]	$\varepsilon_L^+ = 0.06$, $\varepsilon_L^- = -0.06$
Thermoelastic modulus	[MPa/°C]	$\Theta = 0.55$
Transformation temperatures	[°C]	$M_f = 0$, $M_s = 10$, $A_s = 20$, $A_f = 30$

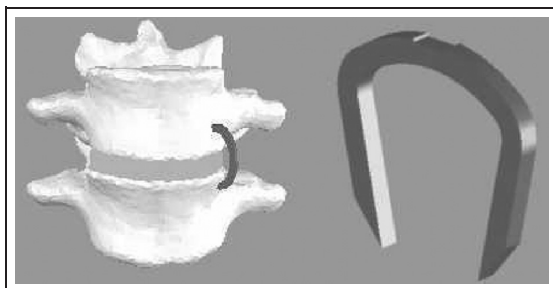


Figure 13. Nitinol SMA staple (Jaber et al., 2008).
SMA: shape memory alloy.

predictions with experimental data shows a good qualitative correlation. Moreover, we implement the proposed model into a UMAT in the commercial nonlinear finite element software ABAQUS and use 2D Euler–Bernoulli beam element to simulate beam problems. These simulations verify that the proposed asymmetric SMA constitutive model is capable of capturing the features of SMAs. Moreover, the results of the simulations show good agreement with the experimental data available in the literature.

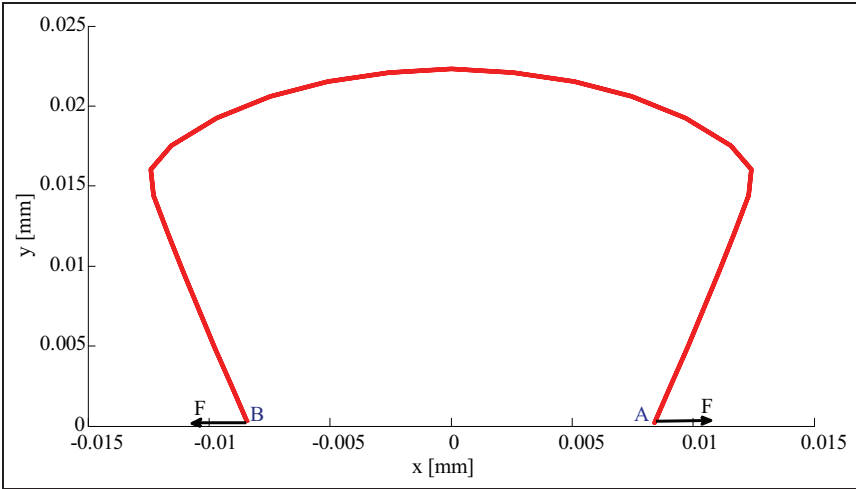


Figure 14. Staple geometry and load direction.

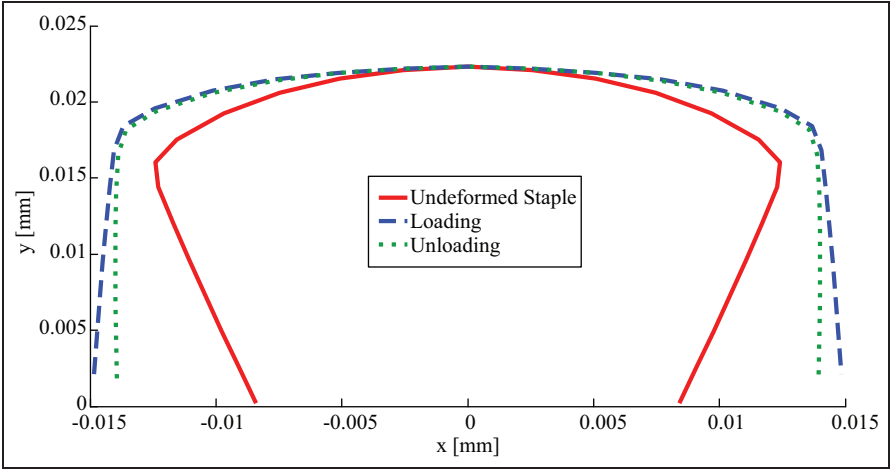


Figure 15. Undeformed, after loading and after unloading geometries of the staple.

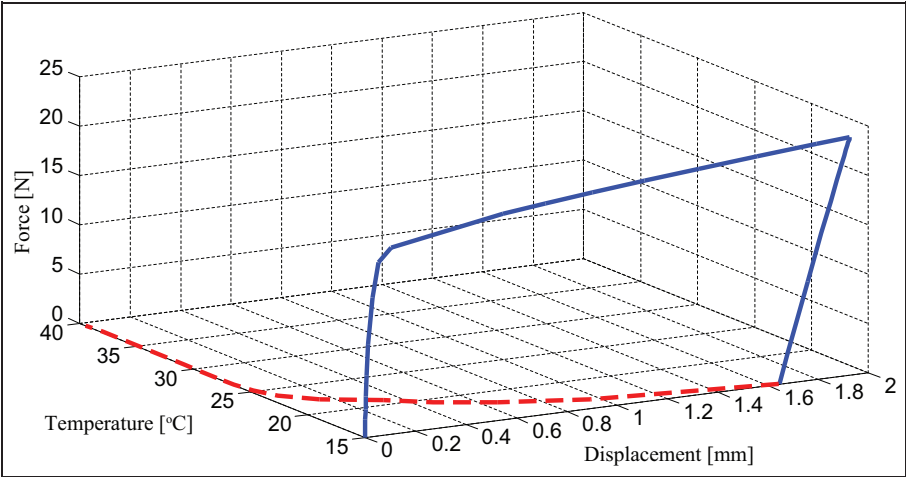


Figure 16. Force-displacement-temperature diagram (at point A shown in Figure 14), the red broken line indicates shape recovery by heating.

Declaration of conflicting interests

The authors declared no potential conflicts of interest with respect to the research, authorship, and/or publication of this article.

Funding

The study was funded by Iran National Science Foundation (INSF) through the project number 89001639.

Notes

1. In this article, a modified transformation kinetics formula presented by Chung et al. (2007) and Khandelwal and Buravalla (2007) has been implemented in the original model proposed by Brinson (1993). The modified equations are then presented in Table 1.
2. As expected, at a temperature above A_f , the material should exhibit superelastic behavior. However, in the experimental data reported by Flor et al. (2006), the material does not recover its original shape by unloading at a temperature above A_f .

References

- ABAQUS (2010). *Users Manual* (Version 6.10). Aachen: Dassault Systemes Simulia Corp.
- Arghavani J, Auricchio F, Naghdabadi R, et al. (2010) A 3-D phenomenological constitutive model for shape memory alloys under multiaxial loadings. *International Journal of Plasticity* 26: 976–991.
- Arghavani J, Auricchio F, Naghdabadi R, et al. (2011) An improved, fully symmetric, finite strain phenomenological constitutive model for shape memory alloys. *Finite Elements in Analysis and Design* 47: 166–174.
- Auricchio F (2001) A robust integration-algorithm for a finite-strain shape-memory alloy superelastic model. *International Journal of Plasticity* 17: 971–990.
- Auricchio F and Lubliner J (1997) A uniaxial model for shape memory alloys. *International Journal of Solids and Structures* 34: 3601–3618.
- Auricchio F, Morganti S, Reali A, et al. (2011) Theoretical and experimental study of the shape memory effect of beams in bending conditions. *Journal of Materials Engineering and Performance* 20: 712–718.
- Bekker A and Brinson LC (1998) Phase diagram based description of the hysteresis behavior of shape memory alloys. *Acta Materialia* 46: 3649–3665.
- Brinson LC (1993) One-dimensional constitutive behavior of shape memory alloys: thermomechanical derivation with non-constant material functions and redefined martensite internal variable. *Journal of Intelligent Material Systems and Structures* 4: 229–242.
- Brocca M, Brinson LC and Bazant ZP (2002) Three dimensional constitutive model for shape memory alloys based on microplane model. *Journal of the Mechanics and Physics of Solids* 50: 1051–1077.
- Buravalla V and Khandelwal A (2011) Evolution kinetics in shape memory alloys under arbitrary loading: experiments and modeling. *Mechanics of Materials* 43: 807–823.
- Chung JH, Heo JS and Lee JJ (2007) Implementation strategy for the dual transformation region in the Brinson SMA constitutive model. *Smart Materials and Structures* 16: N1.
- Decastro JA, Melcher KJ, Noebe RD, et al. (2007) Development of a numerical model for high-temperature shape memory alloys. *Smart Materials and Structures* 16: 2080–2090.
- Evangelista V, Marfia S and Sacco E (2009) A 3D SMA constitutive model in the framework of finite strain. *International Journal for Numerical Methods in Engineering* 81: 761–785.
- Flor SD, Urbina C and Ferrando F (2006) Constitutive model of shape memory alloys: theoretical formulation and experimental validation. *Materials Science and Engineering A* 427: 112–122.
- Flor SD, Urbina C and Ferrando F (2011) Asymmetrical bending model for NiTi shape memory wires: numerical simulations and experimental analysis. *Strain* 47: 255–267.
- Fremond M (1996) Shape memory alloy: a thermomechanical macroscopic theory. In: *Cism Courses and Lectures*, vol. 351. Springer, pp. 3–68. Springer Verlag.
- Gall K, Sehitoglu H, Chumlyakov YI, et al. (1999) Tension–compression asymmetry of the stress–strain response in aged single crystal and polycrystalline NiTi. *Acta Materialia* 47: 1203–1217.
- Gillet Y, Patoor E and Berveiller M (1998) Calculation of pseudoelastic elements using a non-symmetrical thermomechanical transformation criterion and associated rule. *Journal of Intelligent Material Systems and Structures* 9: 366–378. Springer Verlag.
- Govindjee S and Kasper EP (1999) Computational aspects of one-dimensional shape memory alloy modeling with phase diagram. *Computer Methods in Applied Mechanics and Engineering* 171: 309–326.
- Jaber MB, Smaoui H and Terriault P (2008) Finite element analysis of a shape memory alloy three-dimensional beam based on a finite strain description. *Smart Materials and Structures* 17: 045005.
- Khandelwal A and Buravalla R (2007) A correction to the Brinson's evolution kinetics for shape memory alloys. *Journal of Intelligent Material Systems and Structures* 19: 43–46.
- Lagoudas DC (2008) *Shape Memory Alloys: Modeling and Engineering Applications*. New York: Springer.
- Liang C and Rogers CA (1990) One-dimensional thermomechanical constitutive relations for shape memory materials. *Journal of Intelligent Material Systems and Structures* 1: 207–234.
- Logan DL (2007) *A First Course in the Finite Element Method*. 4th ed. Thomson Press, Canada.
- Paiva A, Savi MA, Braga AMB, et al. (2005) A constitutive model for shape memory alloys considering tensile–compressive asymmetry and plasticity. *International Journal of Solids and Structures* 42: 3439–3457.
- Souza AC, Mamiya E and Zouain N (1998) Three-dimensional model for solids undergoing stress induced phase transformations. *European Journal of Mechanics A: Solids* 17: 789–806.
- Tanaka K (1986) A thermomechanical sketch of shape memory effect: one-dimensional tensile behavior. *Res Mechanica* 18: 251–263.

- Tokuda M, Ye M, Takakura M, et al. (1999) Thermomechanical behavior of shape memory alloy under complex loading conditions. *International Journal of Plasticity* 15: 223–239.
- Trochu F and Qian YY (1997) Nonlinear finite element simulation of superelastic shape memory alloy parts. *Computers & Structures* 62: 799–810.
- Vigliotti A (2010) Finite element implementation of a multi-variant shape memory alloy model. *Journal of Intelligent Material Systems and Structures* 21: 685–699.
- Wu X, Grummon DS and Pence TJ (1999) Modeling phase fraction shakedown during thermomechanical cycling of shape memory materials. *Materials Science and Engineering A* 273: 245–250.
- Yang S and Xu M (2011) Finite element analysis of 2D SMA beam bending. *Acta Mechanica Sinica* 27: 738–748.
- Zaki W (2010) An approach to modeling tensile–compressive asymmetry for martensitic shape memory alloys. *Smart Materials and Structures* 19: 025009.

Appendix I

Finite element formulation details

The displacement components of the neutral axis ($u_0(x)$ and $v_0(x)$) can be expressed as

$$\begin{Bmatrix} u_0 \\ v_0 \end{Bmatrix} = \begin{bmatrix} N_{T1} & 0 & 0 & N_{T2} & 0 & 0 \\ 0 & N_{B1} & N_{B2} & 0 & N_{B3} & N_{B4} \end{bmatrix} \{d\} \quad (37)$$

where N_{T1} , N_{T2} , N_{B1} , N_{B2} , N_{B3} , and N_{B4} are called the shape functions and $\{d\}$ is nodal displacements vector. The shape functions N_{T1} , N_{T2} , N_{B1} , N_{B2} , N_{B3} , and N_{B4} are expressed as (Logan, 2007)

$$\begin{aligned} N_{T1} &= 1 - \frac{x}{L} & N_{T2} &= \frac{x}{L} \\ N_{B1} &= \frac{1}{L^3} (2x^3 - 3x^2L + L^3) & N_{B2} &= \frac{1}{L^3} (x^3L - 2x^2L^2 + xL^3) \\ N_{B3} &= \frac{1}{L^3} (-2x^3 + 3x^2L) & N_{B4} &= \frac{1}{L^3} (x^3L - x^2L^2) \end{aligned} \quad (38)$$

where L is the length of the beam element. In addition, $\{d\}$ is nodal displacements vector

$$\{d\}^T = [d_{1x} \quad d_{1y} \quad \phi_{1z} \quad d_{2x} \quad d_{2y} \quad \phi_{2z}] \quad (39)$$

Substitution of equations (38) and (39) into equation (37) and the results into equation (30) yields

$$\begin{aligned} \varepsilon &= - \left[\frac{1}{L} \quad y \frac{12x-6L}{L^3} \quad y \frac{6xL-4L^2}{L^3} \quad -\frac{1}{L} \quad y \frac{-12x+6L}{L^3} \quad y \frac{6xL-2L^2}{L^3} \right] \\ \{d\} &= B\{d\} \end{aligned} \quad (40)$$

We now employ the virtual work principle

$$\delta W_i - \delta W_e = 0 \quad (41)$$

where

$$\delta W_e = \int_V \delta\{d\}^T F_V dV + \int_S \delta\{d\}^T F_S dS \quad (42)$$

$$\delta W_i = \int_V \delta \varepsilon^T \sigma dV \quad (43)$$

where F_V and F_S are, respectively, body forces and surface loading on the element. Substituting equation (40) into equation (43), we obtain

$$\delta W_i = \int_V \delta\{d\}^T B^T \sigma dV = \delta\{d\}^T f^{int} \quad (44)$$

The internal force f^{int} can be expressed as

$$f^{int} = \int_V B^T \sigma dV \quad (45)$$

Thus, using equations (42) to (45), we can simplify equation (41) as

$$f^{int} - f^{ext} = \int_V B^T \sigma dV - \int_V F_V dV - \int_S F_S dS = 0 \quad (46)$$

where f^{ext} is external force. Equation (46) is a nonlinear equation that is usually solved by Newton–Raphson method. To this end, we obtain the stiffness matrix as follows:

$$K = \frac{\partial f^{int}}{\partial \{d\}} = \frac{\partial \left(\int_V B^T \sigma dV \right)}{\partial \{d\}} = \int_V B^T \frac{\partial \sigma}{\partial \{d\}} dV \quad (47)$$

We now use the chain rule to obtain

$$\frac{\partial \sigma}{\partial \{d\}} = \frac{\partial \sigma}{\partial \varepsilon} \frac{\partial \varepsilon}{\partial \{d\}} = \frac{\partial \sigma}{\partial \varepsilon} B \quad (48)$$

Substituting equation (48) into equation (47), the stiffness matrix can be expressed as

$$K = \int_V B^T C B dV \quad (49)$$

where C denotes the tangent matrix

$$C = \frac{d\sigma}{d\varepsilon} \quad (50)$$